



Conditioned structure functions in turbulent hydrogen/air flames

Downloaded from: <https://research.chalmers.se>, 2025-12-05 03:28 UTC

Citation for the original published paper (version of record):

Sabelnikov, V., Lipatnikov, A., Nikolay, N. et al (2022). Conditioned structure functions in turbulent hydrogen/air flames. *Physics of Fluids*, 34(8). <http://dx.doi.org/10.1063/5.0096509>

N.B. When citing this work, cite the original published paper.

Conditioned structure functions in turbulent hydrogen/air flames

Vladimir A. Sabelnikov^{a,*}, Andrei N. Lipatnikov^b, Nikolay V. Nikitin^c,
Francisco E. Hernández-Pérez^d, Hong G. Im^d

^aONERA – The French Aerospace Laboratory, F-91761 Palaiseau, France

^bDepartment of Mechanics and Maritime Sciences, Chalmers University of Technology, Gothenburg, 41296 Sweden

^cLomonosov Moscow State University, Moscow, Russian Federation

^dClean Combustion Research Center, King Abdullah University of Science and Technology,
Thuwal 23955-6900, Saudi Arabia

*Corresponding author, sabelnikov@free.fr

Abstract

Direct numerical simulation data obtained from two turbulent, lean hydrogen-air flames propagating in a box are analyzed to explore the influence of combustion-induced thermal expansion on turbulence in unburned gas. For this purpose, Helmholtz-Hodge decomposition is applied to the computed velocity fields. Subsequently, the second-order structure functions conditioned to unburned reactants are sampled from divergence-free solenoidal velocity field or irrotational potential velocity field, yielded by the decomposition. Results show that thermal expansion significantly affects the conditioned potential structure functions not only inside the mean flame brushes, but also upstream of them. Upstream of the flames, firstly, transverse structure functions for transverse potential velocities grow with distance r between sampling points more slowly when compared to the counterpart structure functions sampled from the entire or solenoidal velocity field. Secondly, the former growth rate depends substantially on the distance from the flame-brush leading edge, even at small r . Thirdly, potential root-mean-square (rms) velocities increase with decreasing distance from the flame-brush leading edge and are comparable with solenoidal rms velocities near the leading edge. Fourthly, although the conditioned axial and transverse potential rms velocities are always close to one another, thus, implying isotropy of the potential velocity field in unburned reactants; the potential structure functions exhibit a high degree of anisotropy. Fifthly, thermal expansion effects are substantial even for the solenoidal structure functions and even upstream of a highly turbulent flame. These findings call for development of advanced models of turbulence in flames, which allow for the discussed thermal expansion effects.

Keywords: Turbulent combustion; Thermal expansion; Helmholtz-Hodge decomposition; Structure functions

32 I. INTRODUCTION

33 Substantial influence of combustion-induced thermal expansion on turbulence in flames has
 34 been known since the seminal papers by Karlovitz et al.¹ and Scurlock and Grover.² Over the
 35 past two decades, rapid development of Direct Numerical Simulation (DNS) methods and
 36 tools allowed researchers³⁻⁹ to reveal various manifestations of this influence and to document
 37 significant changes of basic features of turbulence in premixed flames. Such results reviewed
 38 elsewhere¹⁰⁻¹³ call for revisiting the problem of modeling turbulence in reacting flows.
 39 Although some DNS data indicate that certain combustion-induced thermal expansion effects
 40 are weakly pronounced in highly turbulent flames,¹⁴⁻²¹ these data do not deny the need for
 41 advancing models of turbulence in flames. Indeed, firstly, there is no widely recognized
 42 criterion for assessing importance of the combustion-induced thermal expansion effects under
 43 specific conditions. Secondly, weak influence of the thermal expansion on certain turbulence
 44 characteristics does not prove that all other turbulence characteristics are also weakly affected
 45 by the thermal expansion under the same conditions. For instance, recent experimental
 46 data^{22,23} obtained from highly turbulent lean methane-air swirl flames show importance of
 47 thermal expansion effects such as vorticity generation due to baroclinic torque²² or back-
 48 scatter.²³

49 Thus, there is a clear need for development of an advanced model of turbulence in flames,
 50 which could predict phenomena revealed recently and reviewed elsewhere.¹⁰⁻¹³ However, no
 51 comprehensive modeling framework to represent distinct roles of thermal expansion on
 52 turbulence exists today. To develop such a framework, more knowledge about the influence
 53 of combustion-induced thermal expansion on turbulence is required first. For this reason, a
 54 set of methods applied to explore this influence was greatly extended recently.^{10-13,17-21} In
 55 particular, the joint use of conditioned structure function (SF) techniques^{17,24-26} and Helmholtz-

Hodge decomposition²⁷ (HHD) appears to be a promising tool for acquiring fundamental knowledge on turbulence in flames. The present work aims at applying this newly introduced research tool²⁸ to DNS data of two turbulent lean H₂/air flames with detailed chemistry.^{21,29-31}

In the next section, research methods are presented. Results are reported and discussed in Sect. III, followed by conclusions.

II. RESEARCH METHODS

A. Helmholtz-Hodge decomposition

HHD is a decomposition of a fluctuating velocity field $\mathbf{u}'(\mathbf{x}, t)$ into two subfields: (i) divergence-free solenoidal subfield $\mathbf{u}'_s(\mathbf{x}, t)$ and (ii) curl-free potential subfield $\mathbf{u}'_p(\mathbf{x}, t)$, i.e.,

$$\mathbf{u}' = \mathbf{u}'_s + \mathbf{u}'_p, \quad \nabla \cdot \mathbf{u}'_s = 0, \quad \nabla \times \mathbf{u}'_p = 0. \quad (1)$$

The last equality holds if $\mathbf{u}'_p = \nabla \varphi$, where $\varphi(\mathbf{x}, t)$ is an arbitrary scalar function with $\Delta \varphi = \nabla \cdot \mathbf{u}'_p = \nabla \cdot \mathbf{u}'$ due to Eq. (1). HHD is of particular value for exploring the influence of thermal expansion on the generation of potential velocity fluctuations in flames.

In the present work, two HHD methods were used: (i) conventional HHD²⁷ and (ii) natural decomposition.^{32,33} The former decomposition invokes the following constraint

$$\iiint_V \mathbf{u}'_s \cdot \mathbf{u}'_p d\mathbf{x} = 0, \quad (2)$$

which guarantees the additivity of the bulk kinetic energies of the solenoidal and potential flow fields, i.e.

$$\iiint_V \mathbf{u}' \cdot \mathbf{u}' d\mathbf{x} = \iiint_V \mathbf{u}'_s \cdot \mathbf{u}'_s d\mathbf{x} + \iiint_V \mathbf{u}'_p \cdot \mathbf{u}'_p d\mathbf{x}. \quad (3)$$

Here, V designates the computational domain. Substitution of Eq. (1) into Eq. (2) yields

$$\iiint_V \mathbf{u}'_s \cdot \nabla \varphi d\mathbf{x} = \iiint_V \nabla(\varphi \mathbf{u}'_s) d\mathbf{x} \quad (4)$$

$$- \iiint_V \varphi \nabla \cdot \mathbf{u}'_s d\mathbf{x} = \oint_S \varphi \mathbf{u}'_s \cdot \mathbf{n} dS - \iiint_V \varphi \nabla \cdot \mathbf{u}'_s d\mathbf{x}.$$

74 Here, S is the boundary of the domain V and the unit vector \mathbf{n} is normal to this boundary. The
75 second (volume) integral vanishes, because $\nabla \cdot \mathbf{u}_s = 0$. The first (surface) integral vanishes if
76 $\mathbf{u}_s \cdot \mathbf{n} = 0$. In this case, Eq. (2) holds and

$$\left. \frac{\partial \varphi}{\partial n} \right|_S = \mathbf{n} \cdot \nabla \varphi|_S = \mathbf{n} \cdot \mathbf{u}|_S \quad (5)$$

77 on the boundary S . The Neumann problem given by $\Delta \varphi = \nabla \cdot \mathbf{u}'$ and Eq. (5) has a unique
78 solution for $\varphi(\mathbf{x}, t)$, i.e., the use of Eq. (2) or (5) makes the HHD unique.

79 The natural decomposition^{32,33} deals with an extra vector-field $\mathbf{w}(\mathbf{x}, t)$, defined as follows:

80 (i) $\mathbf{w}(\mathbf{x}, t) = \mathbf{u}(\mathbf{x}, t)$ for all $\mathbf{x} \in V$, and (ii) $\mathbf{w}(\mathbf{x}, t)$ is extrapolated to the entire 3D space \mathbb{R}^3
81 such that $|\mathbf{w}(\mathbf{x}, t)| \rightarrow 0$ for $|\mathbf{x}| \rightarrow \infty$. This velocity field $\mathbf{w}(\mathbf{x}, t)$ can be decomposed in the
82 entire space, i.e.,

$$\mathbf{w} = \nabla \Gamma + \nabla \times \mathbf{S}, \quad \mathbf{x} \in \mathbb{R}^3, \quad (6)$$

$$\Delta \Gamma = \nabla \cdot \mathbf{w}, \quad \mathbf{x} \in \mathbb{R}^3, \quad (7)$$

$$\nabla \times \nabla \times \mathbf{S} = \nabla \times \mathbf{w}, \quad \mathbf{x} \in \mathbb{R}^3. \quad (8)$$

83 Solutions to Eqs. (7)-(8) are unique

$$\Gamma(\mathbf{x}_0, t) = \iiint_{\mathbb{R}^3} G_\infty(\mathbf{x}, \mathbf{x}_0) \nabla \cdot \mathbf{w}(\mathbf{x}, t) d\mathbf{x}, \quad \mathbf{x}_0, \mathbf{x} \in \mathbb{R}^3, \quad (9)$$

$$\mathbf{S}(\mathbf{x}_0, t) = - \iiint_{\mathbb{R}^3} G_\infty(\mathbf{x}, \mathbf{x}_0) \nabla \times \mathbf{w}(\mathbf{x}, t) d\mathbf{x}, \quad \mathbf{x}_0, \mathbf{x} \in \mathbb{R}^3. \quad (10)$$

84 where $G_\infty(\mathbf{x}, \mathbf{x}_0) = -1/(4\pi|\mathbf{x} - \mathbf{x}_0|)$ is the free-space Green's function in \mathbb{R}^3 . Then,
85 integration in Eqs. (9)-(10) can be truncated outside the domain V by interpreting the
86 truncated integrals to be an external influence. Therefore,

$$\Gamma^*(\mathbf{x}_0, t) = \iiint_V G_\infty(\mathbf{x}, \mathbf{x}_0) \nabla \cdot \mathbf{u}(\mathbf{x}, t) d\mathbf{x}, \quad \mathbf{x}_0, \mathbf{x} \in V, \quad (11)$$

$$\mathbf{S}^*(\mathbf{x}_0, t) = - \iiint_V G_\infty(\mathbf{x}, \mathbf{x}_0) \nabla \times \mathbf{u}(\mathbf{x}, t) d\mathbf{x}, \quad \mathbf{x}_0, \mathbf{x} \in V. \quad (12)$$

87 Equation (1) with $\mathbf{u}_s = \nabla \times \mathbf{S}^*$ and $\mathbf{u}_p = \nabla \Gamma^*$ holds due to Eqs. (6)-(8).

88 Results yielded by the two HHD methods were compared in detail in an earlier paper.²⁸
89 Since these results are hardly distinguishable within flame brushes, we will report results
90 obtained using the conventional HHD only.

91 B. Conditioned structure functions

92 In fluid mechanics, the second-order SFs of a velocity field form the following tensor³⁵

$$D_{ij}(\mathbf{x}, \mathbf{r}) \equiv \overline{[u_i(\mathbf{x} + \mathbf{r}, t) - u_i(\mathbf{x}, t)][u_j(\mathbf{x} + \mathbf{r}, t) - u_j(\mathbf{x}, t)]}, \quad (13)$$

93 where overbar designates averaging; u_i and u_j are i -th and j -th components, respectively, of
94 the velocity vector $\mathbf{u} = \{u, v, w\}$. Similarly to the turbulence spectrum, such SFs characterize
95 the distribution of turbulent energy over spatial scales.³⁵ Accordingly, the SFs are widely used
96 to study turbulence since a seminal work by Kolmogorov³⁶ and to model unresolved small-
97 scale effects in Large Eddy Simulations.³⁷

98 When Eq. (13) is applied to a flame, the velocity differences are controlled not only by
99 turbulence, but also by thermal expansion effects. Such effects can be of primary importance
100 if the local flame front is between the points \mathbf{x} and $\mathbf{x} + \mathbf{r}$. Therefore, additional considerations
101 are needed to use SFs in combustion research. To this end, conditioned SFs were

independently introduced by Whitman et al.¹⁷ and by Sabelnikov et al.^{24,25} They applied two different methods to DNS data of highly¹⁷ and weakly^{24,25} turbulent single-step chemistry flames. Subsequently, the latter method was adopted²⁶ to analyze DNS data of single-step chemistry flames, characterized by various ratios $1 \leq u'/S_L \leq 10$ of root-mean-square (rms) velocity, u' , to the laminar flame speed, S_L . Later, conditioned SFs were jointly used with HHD²⁸ to explore thermal expansion effects in weakly turbulent single-step chemistry flames. Yet, neither application of conditioned SFs to complex chemistry turbulent flames nor joint application of conditioned SFs and HHD to moderately or highly turbulent combustion has been reported.

Here, the conditioned second-order SFs of the velocity field are defined as follows^{24,25}

$$D_{ij}^{\alpha\beta}(\mathbf{x}, \mathbf{r}) \equiv \frac{1}{P_{\alpha\beta}} \overline{[u_i(\mathbf{x} + \mathbf{r}, t) - u_i(\mathbf{x}, t)][u_j(\mathbf{x} + \mathbf{r}, t) - u_j(\mathbf{x}, t)]I_\alpha(\mathbf{x}, t)I_\beta(\mathbf{x} + \mathbf{r}, t)}, \quad (14)$$

where superscripts α and β refer to the mixture state; the indicator function $I_u(\mathbf{x}, t)$ is equal to unity if reactants are observed in point \mathbf{x} at instant t and vanishes otherwise; $I_b(\mathbf{x}, t) = 1$ if products are observed in point \mathbf{x} at instant t and vanishes otherwise; $I_r(\mathbf{x}) = 1$ if $I_u(\mathbf{x}, t) = I_b(\mathbf{x}, t) = 0$ and vanishes otherwise; and $P_{\alpha\beta} = \overline{I_\alpha(\mathbf{x}, t)I_\beta(\mathbf{x} + \mathbf{r}, t)}$ are probabilities that the mixture states α and β are recorded in points \mathbf{x} and $\mathbf{x} + \mathbf{r}$, respectively, at the same instant.

Depending on α and β , there are different conditioned SF tensors, with $D_{ij}(\mathbf{x}, \mathbf{r})$ being equal to $\sum_{\alpha=1}^3 \sum_{\beta=1}^3 D_{ij}^{\alpha\beta}(\mathbf{x}, \mathbf{r})$ due to the identity of $\sum_{\alpha=1}^3 \sum_{\beta=1}^3 I_\alpha(\mathbf{x})I_\beta(\mathbf{x} + \mathbf{r}) = 1$. The present work is restricted to the conditioned SFs D_{ij}^{uu} sampled in the cases where both \mathbf{x} and $\mathbf{x} + \mathbf{r}$ are in the unburned gas. Such conditioned SFs appear to be of the most interest because (i) a flame propagates into unburned gas and (ii) the velocity field upstream of the flame plays a key role in the flame acceleration. Henceforth, the superscript uu will be omitted for brevity.

124 Since the DNS data analyzed here were obtained from statistically one-dimensional and
125 planar flames propagating from right to left along the x -direction in a box, the flow field is
126 assumed to be statistically isotropic and homogeneous in any plane $x = \text{const}$. Hence, the
127 present study is restricted to SFs found for points $\mathbf{x} = \{x, y, z\}$ and $\mathbf{x} = \{x, y + r_y, z + r_z\}$ that
128 belong to the same transverse plane $x = \text{const}$, i.e., $\mathbf{r} = \{0, r_y, r_z\}$.

129 C. Numerical simulations and data analysis

130 As the DNS were discussed earlier,²⁹⁻³¹ only a brief description is given here. Lean (the
131 equivalence ratio $\Phi=0.7$) H_2 -air turbulent flames propagating in a box were investigated by
132 (i) adopting a detailed (9 species, 23 reversible reactions) chemical mechanism³⁸ with the
133 mixture-averaged transport model and (ii) numerically solving unsteady three-dimensional
134 governing equations written in compressible form.

135 Along the flame propagation direction x , inflow and outflow characteristic boundary
136 conditions were set. Other boundaries were periodic. A divergence-free, isotropic,
137 homogeneous turbulent velocity field was generated using a pseudo spectral method³⁹ and
138 adopting the Passot-Pouquet spectrum.⁴⁰ The field was injected through the inlet (left)
139 boundary and decayed along the mean flow direction (x -axis).

140 **TABLE I.** Relevant parameters characterizing the DNS cases

	u'/S_L	L_T/δ_L	Re_T	Da	Ka_1	Ka_2
W	0.7	14	227	20	33	0.5
H	5.0	14	1623	2.8	270	4

141 Ratios of the inflow value of the rms velocity to S_L , ratios of the most energetic length scale
142 L_T of the Passot-Pouquet spectrum to the laminar flame thickness $\delta_L = (T_b - T_u)/\max|\nabla T|$,
143 turbulent Reynolds number $Re_T = u'L_T/\nu_u$, Damköhler number $Da = L_TS_L/(u'\delta_L)$, and
144 two Karlovitz numbers are reported for the studied flames in Table 1. Here, $S_L = 1.36$ m/s

145 and $\delta_L = 0.36$ mm have been computed using the same chemical mechanism under the
146 simulation conditions (temperature $T_u = 300$ K and pressure $P = 1$ atm); ν_u is the kinematic
147 viscosity of unburned gas; $Ka_1 = (\delta_L/\eta_K)^2$ and $Ka_2 = \delta_L/(S_L\tau_K)$ have been evaluated
148 using (i) the Kolmogorov length scale $\eta_K = \nu_u^{3/4}\bar{\epsilon}^{-1/4}$ and time scale $\tau_K = \nu_u^{1/2}\bar{\epsilon}^{-1/2}$, (ii)
149 the dissipation rate $\bar{\epsilon} = 2\nu_u\overline{S_{ik}S_{ik}}$ averaged over the leading edge ($\bar{c} = 0.01$, with the
150 combustion progress variable c being defined using fuel mass fraction) of the mean flame
151 brush, and (iii) the rate-of-strain tensor $S_{ik} = 0.5(\partial u_i/\partial x_k + \partial u_k/\partial x_i)$.

152 The number Ka_1 is significantly larger than Ka_2 , because $\delta_L = (T_b - T_u)/\max|\nabla T| \gg$
153 ν_u/S_L for the lean hydrogen-air laminar flame addressed here. Since (i) thicknesses of preheat
154 and reaction zones are comparable in this flame and (ii) Ka_1 is large; both cases W and H are
155 associated with a significant probability of penetration of small-scale turbulent eddies into
156 local reaction zones.⁴¹ Since $Ka_2 > 1$ in flame H, it is also associated with substantial
157 probability of local combustion quenching.⁴¹ Thus, as far as the influence of turbulence on
158 combustion is concerned, case H is definitely associated with highly turbulent burning.
159 Nevertheless, even in this case, the influence of combustion on turbulence can be significant,
160 as shown in Sect. III.

161 When analyzing the DNS data, firstly, transverse-averaged quantities $\langle q \rangle(x, t)$ were
162 sampled at each instant. Secondly, these x -dependencies were mapped to $\langle c \rangle$ -dependencies
163 using the averaged profiles $\langle c \rangle(x, t)$. Thirdly, mean values $\bar{q}(\bar{c})$ of the quantity q , e.g., a
164 product of velocity differences in Eq. (14), were found by averaging $\langle q \rangle[\langle c \rangle(x, t)]$ over time.

165 The probability $P_{uu}(x, r)$ and the conditioned SFs determined by Eq. (14) were sampled
166 from points characterized by $c(\mathbf{x}, t) < \epsilon \ll 1$, with three such SFs being considered. Firstly,
167 the transverse SFs $D_{xx,T}(x, r)$ for the axial velocity u' were computed by sampling
168 $[u'(\mathbf{x} + \mathbf{r}, t) - u'(\mathbf{x}, t)]^2$ from two sets of points: (i) $\mathbf{r} = \{0, r, 0\}$ and (ii) $\mathbf{r} = \{0, 0, r\}$.

169 Subsequently, the two samples were averaged. Secondly, the transverse SFs $D_{yz,T}(x, r)$ for
170 the transverse velocities v and w were obtained by sampling (i) $[v'(\mathbf{x} + \mathbf{r}, t) - v'(\mathbf{x}, t)]^2$
171 from points characterized by $\mathbf{r} = \{0, 0, r\}$ and (ii) $[w'(\mathbf{x} + \mathbf{r}, t) - w'(\mathbf{x}, t)]^2$ from points
172 characterized by $\mathbf{r} = \{0, r, 0\}$. Subsequently, the two samples were averaged. Thirdly, the
173 longitudinal SFs $D_{yz,L}(x, r)$ for the transverse velocities were found by sampling (i)
174 $[v'(\mathbf{x} + \mathbf{r}, t) - v'(\mathbf{x}, t)]^2$ from points characterized by $\mathbf{r} = \{0, r, 0\}$ and (ii) $[w'(\mathbf{x} + \mathbf{r}, t) -$
175 $w'(\mathbf{x}, t)]^2$ from points characterized by $\mathbf{r} = \{0, 0, r\}$. Subsequently, the two samples were
176 averaged. Solenoidal and potential conditioned SFs were obtained by separately applying such
177 diagnostics to the solenoidal and potential velocity subfields, respectively.

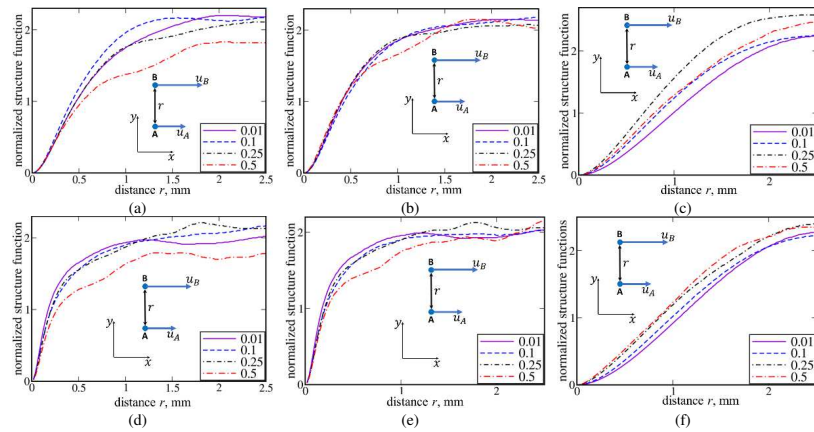
178 Reported in the following are dependencies of the conditioned SFs on the distance r ,
179 sampled either inside a flame brush at various $\bar{c}(x)$ or upstream of a flame brush at various
180 distances Δx from it. The SFs were sampled adopting the threshold $\epsilon = 0.05$ and the
181 combustion progress variable $c = 1 - Y_F/Y_{F,u}$ defined using fuel mass fraction. Weak
182 sensitivity of the obtained results to ϵ (either 0.01 or 0.05) or to the choice of combustion
183 progress variable (temperature, water, and oxygen-based combustion progress variables were
184 also adopted to analyze the same DNS data³⁰) was checked.

185 III. RESULTS AND DISCUSSION

186 Figure 1 shows normalized transverse SFs $D_{xx,T}[\bar{c}(x), r]$ for the total, solenoidal, and
187 potential fluctuating axial velocity fields, conditioned to unburned gas in flames W (top row)
188 and H (bottom row). The SFs have been sampled from various transverse planes characterized
189 by different \bar{c} (see the figure legends). Henceforth, (i) each subfigure that reports a SF
190 contains an insert, which sketches the SF type, and (ii) total, solenoidal, and potential SFs are

191 normalized using conditioned total, solenoidal, and potential rms velocities, respectively,
192 which are reported in Fig. 2.

193 At first glance, Figs. 1a and 1d do not show any significant and systematic change of the
194 total SF $D_{xx,T}[\bar{c}(x), r]$ with \bar{c} if $\bar{c} \leq 0.25$. Such changes are not observed for the solenoidal
195 SFs either (Figs. 1b and 1e). Concerning the differences between $D_{xx,T}[\bar{c}(x), r]$ sampled at
196 $\bar{c} \leq 0.25$ and $\bar{c} = 0.5$ (red dotted-dashed lines), they can be attributed to decorrelation of
197 unburned gas motion in two points on the opposite sides of a flame segment. The probability
198 of finding such pairs of points is increased with the distance r and with \bar{c} , thus, making the
199 $D_{xx,T}[\bar{c} = 0.5, r]$ -curves less smooth at $r > \delta_L$.



200 **FIG. 1.** Normalized transverse structure functions for the axial velocity, conditioned to unburned gas
201 and sampled from different transverse planes in flames W (top row) and H (bottom row). Values of
202 Reynolds-averaged combustion progress variable characterizing sampling planes are reported in the
203 legends. Results obtained by analyzing (a) and (d) total, (b) and (e) solenoidal, or (c) and (f) potential
204 velocity fields are reported in the left, middle, and right columns, respectively. $\delta_L = 0.36$ mm.

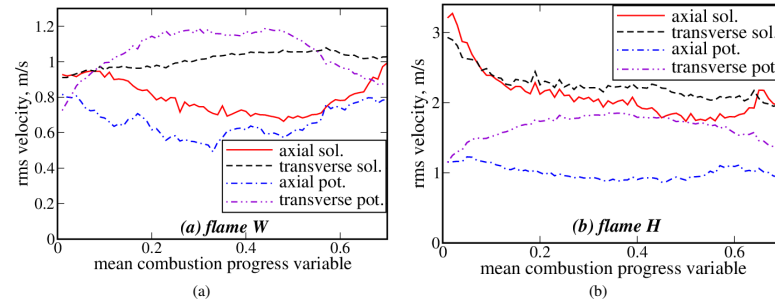


FIG. 2. Variations of conditioned (i) axial solenoidal and potential rms velocities $\langle u_s'^2 | c(\mathbf{x}, t) < 0.05 \rangle^{1/2}$ and $\langle u_p'^2 | c(\mathbf{x}, t) < 0.05 \rangle^{1/2}$, respectively, and (ii) transverse solenoidal and potential rms velocities $\langle 0.5(v_s'^2 + w_s'^2) | c(\mathbf{x}, t) < 0.05 \rangle^{1/2}$ and $\langle 0.5(v_p'^2 + w_p'^2) | c(\mathbf{x}, t) < 0.05 \rangle^{1/2}$, respectively, in flames (a) W and (b) H.

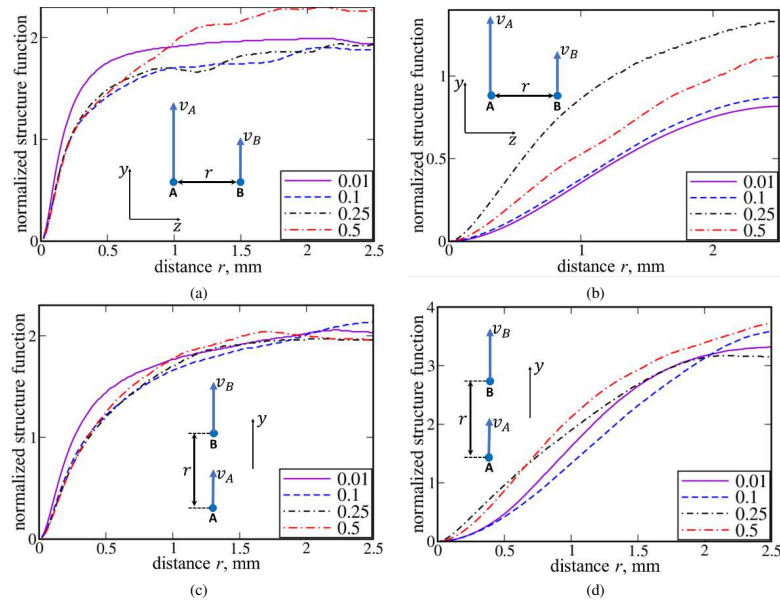


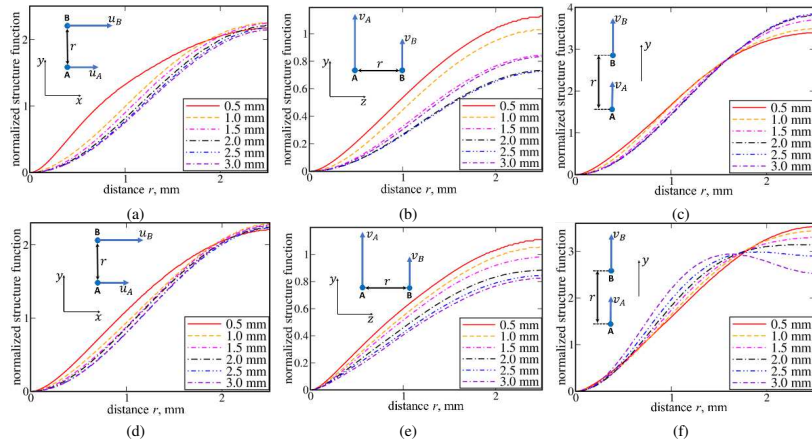
FIG. 3. Normalized (a) and (b) transverse structure functions $D_{yz,T}[\bar{c}(x), r]$ (top row) or (c) and (d) longitudinal structure functions $D_{yz,L}[\bar{c}(x), r]$ (bottom row) for the transverse velocities, conditioned to unburned gas and sampled from different transverse planes in flame H. Values of Reynolds-averaged combustion progress variable characterizing sampling planes are reported in the legends. Results obtained by analyzing (a) and (c) total or (b) and (d) potential fluctuating velocity fields are reported in the left and right columns, respectively. $\delta_L = 0.36$ mm.

215 On the contrary, the potential SF $D_{xx,T}[\bar{c}(x), r]$ is increased with \bar{c} at $\bar{c} \leq 0.25$ (Figs. 1c
216 and 1f). The trend is well pronounced in case W (Fig. 1c). Even in the highly turbulent flame
217 H (Fig. 1f), the trend is evident, but variations in $D_{xx,T}[\bar{c}(x), r]$ with \bar{c} are less pronounced,
218 thus indicating some reduction of the magnitude of thermal expansion effects in more intense
219 turbulence. Moreover, the increase in the potential SF $D_{xx,T}[\bar{c}(x), r]$ with \bar{c} (at $\bar{c} \leq 0.25$) is
220 evident at various distances r , including small distances $r < \delta_L$. Thus, Figs. 1c and 1f clearly
221 indicate substantial influence of combustion-induced thermal expansion on all scales of
222 potential velocity fluctuations in unburned gas within the mean flame brush. While the
223 potential SFs are normalized using the potential rms velocities, Fig. 2 shows that the potential
224 and solenoidal axial rms velocities are comparable in magnitude in flame W or H.

225 Significant variations of the conditioned potential SFs $D_{yz,T}[\bar{c}(x), r]$ and $D_{yz,L}[\bar{c}(x), r]$
226 with \bar{c} are also seen in both cases, including the highly turbulent flame H (see Figs. 3b and
227 3d, where such variations are strongly pronounced for $0.1 \leq \bar{c} \leq 0.25$, especially for
228 $D_{yz,T}[\bar{c}(x), r]$). Again, differences between the conditioned potential SFs $D_{yz,T}[\bar{c}(x), r]$ or
229 $D_{yz,L}[\bar{c}(x), r]$ sampled at different \bar{c} are significant even at small distance $r < \delta_L$. Moreover,
230 comparison of Figs. 3a and 3b or Figs. 3c and 3d shows an important qualitative difference
231 between the total (left column in Fig. 3) and potential (right column) SFs; the potential SFs
232 increase significantly slower with distance r and do not level off even at large r . The same
233 qualitative difference is observed when comparing Figs. 1a and 1c or Figs. 1d and 1f.

234 As shown above, the spatial structure of potential velocity fluctuations differs substantially
235 from that of the incoming solenoidal turbulent fluctuations. Such changes of the spatial
236 structure of the fluctuating velocity field in unburned gas within flame brush are not
237 negligible, because conditioned solenoidal and potential rms velocities are of the same order
238 even in the highly turbulent flame H (Fig. 2b). Also note that the conditioned total SFs

239 $D_{yz,T}[\bar{c}(x), r]$ and $D_{yz,L}[\bar{c}(x), r]$ sampled at $\bar{c} = 0.01$ differ from their counterparts sampled
240 at $0.1 \leq \bar{c}$, even at small distance $r < \delta_L$ (Figs. 3a and 3c), further indicating the importance
241 of the influence of thermal expansion on turbulence in flames.



242 **FIG. 4.** Normalized potential structure functions (a) and (d) $D_{xx,T}(x, r)$ (left column), (b) and (e)
243 $D_{yz,T}(x, r)$ (middle column), or (c) and (f) $D_{yz,L}(x, r)$ (right column) sampled upstream of flames (a-c)
244 W (top row) and (d-f) H (bottom row) at different distances from their leading edges, specified in
245 the legends. $\delta_L = 0.36$ mm.

246 For the potential velocity field, such an influence is well pronounced even upstream ($\bar{c} <$
247 0.01) of the flame brushes in both cases (Fig. 4), with the field being highly anisotropic.
248 Indeed, on the one hand, variations of potential SFs with the distance Δx (see legends) from
249 the flame leading edge are most pronounced for $D_{yz,T}(x, r)$ (Figs. 4b and 4e) and least
250 pronounced for $D_{yz,L}(x, r)$ (Figs. 4c and 4f). On the other hand, at large r , $D_{yz,L}(x, r)$ is
251 significantly larger than $D_{yz,T}(x, r)$. Moreover, the anisotropy of the potential SFs is
252 significantly more pronounced than the weak anisotropy of potential rms velocities (Fig. 5),
253 which were used to normalize the SFs. This demonstrates that simple diagnostic tools (rms
254 velocities) are unable to reveal the explored thermal expansion effects.

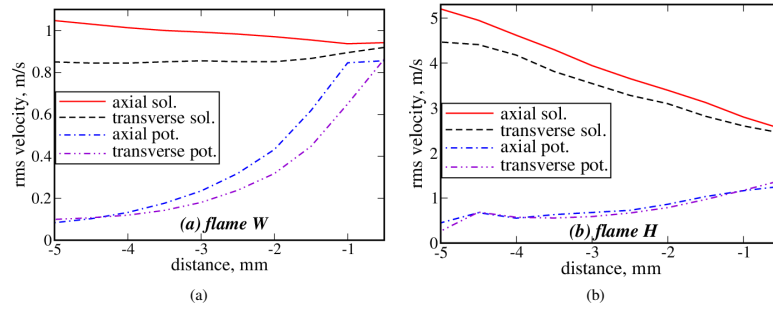


FIG. 5. Variations of (i) axial solenoidal and potential rms velocities $(\overline{u_s'^2})^{1/2}$ and $(\overline{u_p'^2})^{1/2}$, respectively, and (ii) transverse solenoidal and potential rms velocities $[0.5(\overline{v_s'^2} + \overline{w_s'^2})]^{1/2}$ and $[0.5(\overline{v_p'^2} + \overline{w_p'^2})]^{1/2}$, respectively, upstream of flames (a) W and (b) H.

Comparison of Figs. 4a and 4d or 4b and 4e indicates that variations in the potential transverse structure function $D_{xx,T}(x, r)$ or $D_{yz,T}(x, r)$, respectively, with Δx are more pronounced in flame W, thus, again implying some reduction of the magnitude of thermal expansion effects in more intense turbulence. However, comparison of Figs. 4c and 4f shows the opposite trend for the potential longitudinal structure function $D_{yz,L}(x, r)$.

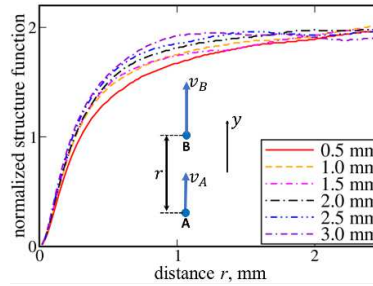
Figure 4 also shows that the potential SFs $D_{yz,T}(x, r)$ and $D_{yz,L}(x, r)$ do not approach 2 at large r . To the contrary, in homogeneous turbulence, $D_{ii}(\mathbf{r}) = 2\overline{u_i'^2}$ at large distances $|\mathbf{r}|$ because the correlation between velocities vanishes.³⁵ Thus, Fig. 4 indicates that combustion-induced transverse velocity fluctuations correlate at large distances. Difference between transverse velocities $v(x, y, z, t)$ and $v(x, y + r, z, t)$ could be statistically positive even at large r , because thermal expansion in a flame tongue can push unburned gas to the opposite directions on the opposite sides of the tongue. As a result, within a flame brush, $D_{yz,L}(x, r)$ could be significantly larger than 2 at large r (Fig. 3d). Figures 4c and 4f imply that such flow perturbations can expand upstream of a flame brush due to pressure waves.

272 Figure 5 shows that, upstream of a flame brush, the potential rms velocity increases with
 273 decreasing distance from the flame leading edge (from left to right), with the effect being more
 274 pronounced in case W. As a result, potential and solenoidal rms velocities are almost equal
 275 or, at least, comparable at $|\Delta x| = 0.5$ mm in case W or H, respectively. While comparable
 276 magnitudes of the potential and solenoidal rms velocities at $|\Delta x| = 0.5$ mm in case H stem
 277 partially from the spatial decay of the solenoidal velocity fluctuations, the Karlovitz numbers
 278 reported in Table 1 have been evaluated using the dissipation rate $\bar{\epsilon}$ sampled at $|\Delta x| = 0$.
 279 Thus, despite the turbulence decay, case H deals with a highly turbulent flame. Moreover,
 280 even if an increase in the potential rms velocities with decreasing $|\Delta x|$ seems to be more
 281 pronounced in flame W, these rms velocities are larger in case H at $|\Delta x| = 0$.

282 The simulated influence of combustion-induced thermal expansion on turbulence upstream
 283 of a premixed flame brush is not unexpected. This effect stems from rapid propagation of
 284 pressure perturbations from the flame to upstream flow of unburned reactants. In a laminar
 285 flow, such pressure perturbations are well known to cause hydrodynamic instability of a
 286 laminar premixed flame,⁴² or self-similar acceleration of a large-scale flame kernel ignited in
 287 a quiescent mixture.⁴³ In turbulent flows, some influence of a premixed flame on upstream
 288 turbulence was documented in a few experimental papers,^{44,45} but the phenomenon requires
 289 more studies. It has not yet been explored by another research group by analyzing DNS data
 290 obtained from premixed turbulent flames or by adopting HHD techniques.

291 Finally, Fig. 6 shows that even solenoidal SFs sampled upstream of flame H vary with the
 292 distance $|\Delta x|$, with the effect being most pronounced at $\delta_L < r < 3\delta_L$ and $|\Delta x| \leq 1$ mm. A
 293 flame can affect the upstream solenoidal velocity field due to the potential velocity
 294 contribution to vortex-stretching term in vorticity transport equation,¹⁰⁻¹³ but such secondary

295 effects are less pronounced than the direct influence of combustion-induced pressure
296 perturbations on the potential velocity.



297
298 **FIG. 6.** Normalized solenoidal structure functions $D_{yz,L}(x, r)$ sampled upstream of flame H.

299 IV. CONCLUSIONS

300 Two advanced research tools, (i) Helmholtz-Hodge decomposition of fluctuating velocity
301 into divergence-free solenoidal and irrotational potential components and (ii) conditioned
302 structure functions, were jointly used to explore the influence of combustion-induced thermal
303 expansion on turbulence by analyzing DNS data of complex chemistry, lean H_2 /air, turbulent
304 flames. While these two methods were earlier²⁸ applied to explore such an influence, the major
305 advancement of the present work consists of showing importance of thermal expansion effects
306 in highly turbulent flames. Moreover, the present analysis has yielded new insights into the
307 influence of thermal expansion on turbulence, as follows.

308 Firstly, results show that thermal expansion effects can seem to be weakly pronounced
309 when analyzing conditioned SFs for the entire or solenoidal velocity field, but well
310 pronounced when exploring potential SFs. Moreover, while the potential SFs clearly show
311 significant anisotropy of velocity field upstream of flame brush, such a trend is not revealed
312 when analyzing the potential rms velocities. Thus, the use of a single diagnostic technique is
313 not sufficient to prove that thermal expansion effects are of minor importance.

314 Secondly, under conditions of the present study, thermal expansion substantially changes
315 not only SFs conditioned to unburned gas within mean flame brush, but also SFs sampled
316 upstream of the flame brush. Such effects are more pronounced for the potential SFs but are
317 also notable for the solenoidal SFs. These results show that a premixed flame is stretched by
318 turbulence that differs substantially from turbulence far upstream of the flame. While the
319 documented effects of combustion-induced thermal expansion on the flow are more
320 pronounced in the flame W associated with a less intense turbulence, they play a role in the
321 highly turbulent flame H as well.

322 The reported findings call for development of advanced models of turbulence in flames,
323 which allow for the discussed thermal expansion effects and can predict them at least
324 qualitatively. The joint use of HHD and conditioned SF methods appears to be a promising
325 tool for acquiring fundamental knowledge that is required for development of such models.
326 Since comparison of the present results obtained from complex-chemistry moderately and
327 highly turbulent flames with results obtained earlier²⁸ from two single-step-chemistry weakly
328 turbulent flames does not reveal any significant effect resulting from complex combustion
329 chemistry, it is recommended to perform future DNS studies of the influence of premixed
330 combustion on turbulence by employing simpler chemical kinetic mechanisms in favor of
331 computational efficiency to cover a wider range of turbulent flame characteristics (u'/S_L ,
332 L_T/δ_L , Ka , Da , Re_T , etc.). On the contrary complex chemistry effects should be addressed
333 when exploring the influence of turbulence on combustion.

334 ACKNOWLEDGEMENTS

335 VAS gratefully acknowledges the financial support provided by ONERA. ANL gratefully
336 acknowledges the financial support provided by Combustion Engine Research Center
337 (CERC). FEHP and HGI were sponsored by King Abdullah University of Science and

338 Technology (KAUST). Computational resources for the DNS calculations were provided by
339 the KAUST Supercomputing Laboratory.

340 AUTHOR DECLARATIONS

341 Conflict of Interest

342 The authors have no conflicts to disclose.

343 DATA AVAILABILITY

344 The data that support the findings of this study are available from the corresponding author
345 upon reasonable request.

346 REFERENCES

- 347 ¹B. Karlovitz, D. W. Denniston, and F. E. Wells, "Investigation of turbulent flames," J. Chem. Phys.
348 **19**, 541 (1951).
- 349 ²A. C. Scurlock and J. H. Grover, "Propagation of turbulent flames," Proc. Combust. Inst. **4**, 645 (1953).
- 350 ³C. Dopazo, L. Cifuentes, and N. Chakraborty, "Vorticity budgets in premixed combustng turbulent
351 flows at different Lewis numbers," Phys. Fluids **29**, 045106 (2017).
- 352 ⁴A. N. Lipatnikov, V. A. Sabelnikov, S. Nishiki, and T. Hasegawa, "Combustion-induced local shear
353 layers within premixed flamelets in weakly turbulent flows," Phys. Fluids **30**, 085101 (2018).
- 354 ⁵A. N. Lipatnikov, V. A. Sabelnikov, S. Nishiki, and T. Hasegawa, "Does flame-generated vorticity
355 increase turbulent burning velocity?" Phys. Fluids **30**, 081702 (2018).
- 356 ⁶A. N. Lipatnikov, V. A. Sabelnikov, S. Nishiki, and T. Hasegawa, "A direct numerical simulation
357 study of the influence of flame-generated vorticity on reaction-zone-surface area in weakly turbulent
358 premixed combustion" Phys. Fluids **31**, 055101 (2019).
- 359 ⁷A. R. Varma, U. Ahmed, and N. Chakraborty "Effects of body forces on vorticity and enstrophy
360 evolutions in turbulent premixed flames," Phys. Fluids **33**, 035102 (2021).
- 361 ⁸J. F. MacArt and M. E. Mueller, "Damköhler number scaling of active cascade effects in turbulent
362 premixed combustion," Phys. Fluids **33**, 035103 (2021).
- 363 ⁹N. Chakraborty, C. Kasten, U. Ahmed, and M. Klein, "Evolutions of strain rate and dissipation rate of
364 kinetic energy in turbulent premixed flames," Phys. Fluids **33**, 125132 (2021).
- 365 ¹⁰A. N. Lipatnikov and J. Chomiak, "Effects of premixed flames on turbulence and turbulent scalar
366 transport," Prog. Energy Combust. Sci. **36**, 1 (2010).
- 367 ¹¹V. A. Sabelnikov and A. N. Lipatnikov, "Recent advances in understanding of thermal expansion
368 effects in premixed turbulent flames," Annu. Rev. Fluid Mech. **49**, 91 (2017).
- 369 ¹²N. Chakraborty, "Influence of thermal expansion on fluid dynamics of turbulent premixed combustion
370 and its modeling implications," Flow Turbul. Combust. **106**, 753 (2021).
- 371 ¹³A. M. Steinberg, P. E. Hamlington, and X. Zhao, "Structure and dynamics of highly turbulent
372 premixed combustion," Prog. Energy Combust. Sci. **85**, 100900 (2021).
- 373 ¹⁴P. E. Hamlington, A. Y. Poludnenko, and E. S. Oran, "Interactions between turbulence and flames in
374 premixed reacting flows," Phys. Fluids **23**, 125111 (2011).
- 375 ¹⁵B. Bobbitt, S. Lapointe, and G. Blanquart, "Vorticity transformation in high Karlovitz number
376 premixed flames," Phys. Fluids **28**, 015101 (2016).

This is the author's peer reviewed, accepted manuscript. However, the online version of record will be different from this version once it has been copyedited and typeset.

PLEASE CITE THIS ARTICLE AS DOI: 10.1063/5.0096509

Accepted to Phys. Fluids 10.1063/5.0096509

- 377 ¹⁶B. Bobbitt and G. Blanquart, "Vorticity isotropy in high Karlovitz number premixed flames," Phys.
378 Fluids **28**, 105101 (2016).
- 379 ¹⁷S. H. R. Whitman, C. A. Z. Towery, A. Y. Poludnenko, and P. E. Hamlington, "Scaling and collapse
380 of conditional velocity structure functions in turbulent premixed flames," Proc. Combust. Inst. **37**,
381 2527 (2019).
- 382 ¹⁸J. Lee, J. F. MacArt, M. E. Mueller, "Heat release effects on the Reynolds stress budgets in turbulent
383 premixed jet flames at low and high Karlovitz numbers," Combust. Flame **216**, 1 (2020).
- 384 ¹⁹R. Darragh, C. A. Z. Towery, A. Y. Poludnenko, and P. E. Hamlington, "Particle pair dispersion and
385 eddy diffusivity in a high-speed premixed flame," Proc. Combust. Inst. **38**, 2845 (2021).
- 386 ²⁰J. Lee and M. E. Mueller, "Closure modeling for the conditional Reynolds stresses in turbulent
387 premixed combustion," Proc. Combust. Inst. **38**, 3031 (2021).
- 388 ²¹V. A. Sabelnikov, A. N. Lipatnikov, S. Nishiki, H. L. Dave, F. E. Hernández-Pérez, W. Song, and H.
389 G. Im, "Dissipation and dilatation rates in premixed turbulent flames," Phys. Fluids **33**, 035112
390 (2021).
- 391 ²²A. Kazbekov and A. M. Steinberg, "Flame- and flow-conditioned vorticity transport in premixed swirl
392 combustion," Proc. Combust. Inst. **38**, 2949 (2021).
- 393 ²³A. Kazbekov and A. M. Steinberg, "Physical space analysis of cross-scale turbulent kinetic energy
394 transfer in premixed swirl flames," Combust. Flame **229**, 111403 (2021).
- 395 ²⁴V. A. Sabelnikov, A. N. Lipatnikov, S. Nishiki, and T. Hasegawa, "Application of conditioned
396 structure functions to exploring influence of premixed combustion on two-point turbulence
397 statistics," Proc. Combust. Inst. **37**, 2433 (2019).
- 398 ²⁵V. A. Sabelnikov, A. N. Lipatnikov, S. Nishiki, and T. Hasegawa, "Investigation of the influence of
399 combustion-induced thermal expansion on two-point turbulence statistics using conditioned
400 structure functions," J. Fluid Mech. **867**, 45 (2019).
- 401 ²⁶P. Brearley, U. Ahmed, N. Chakraborty, and A. Lipatnikov, "Statistical behaviors of conditioned two-
402 point second-order structure functions in turbulent premixed flames in different combustion
403 regimes," Phys. Fluids **31**, 115109 (2019).
- 404 ²⁷A. J. Chorin and J. E. Marsden, *A Mathematical Introduction to Fluid Mechanics* (Springer, Berlin,
405 Germany, 1993).
- 406 ²⁸V. A. Sabelnikov, A. N. Lipatnikov, N. Nikitin, S. Nishiki, and T. Hasegawa, "Application of
407 Helmholtz-Hodge decomposition and conditioned structure functions to exploring influence of
408 premixed combustion on turbulence upstream of the flame," Proc. Combust. Inst. **38**, 3077 (2021).
- 409 ²⁹D. H. Wacks, N. Chakraborty, M. Klein, P. G. Arias, and H. G. Im, "Flow topologies in different
410 regimes of premixed turbulent combustion: A direct numerical simulation analysis," Phys. Rev.
411 Fluids **1**, 083401 (2016).
- 412 ³⁰A. N. Lipatnikov, V. A. Sabelnikov, F. E. Hernández-Pérez, W. Song, and H. G. Im, "A priori DNS
413 study of applicability of flamelet concept to predicting mean concentrations of species in turbulent
414 premixed flames at various Karlovitz numbers," Combust. Flame **222**, 370 (2020).
- 415 ³¹A. N. Lipatnikov, V. A. Sabelnikov, F. E. Hernández-Pérez, W. Song, and H. G. Im, "Prediction of
416 mean radical concentrations in lean hydrogen-air turbulent flames at different Karlovitz numbers
417 adopting a newly extended flamelet-based presumed PDF," Combust. Flame **226**, 248 (2021).
- 418 ³²H. Bhatia, G. Norgard, V. Pascucci, and P.-T. Bremer, "The Helmholtz-Hodge decomposition – a
419 survey," IEEE Trans. Vis. Comput. Graph. **19**, 1386 (2013).
- 420 ³³H. Bhatia, V. Pascucci, and P.-T. Bremer, "The natural Helmholtz-Hodge decomposition for open-
421 boundary flow analysis," IEEE Trans. Vis. Comput. Graph. **20**, 1566 (2014).
- 422 ³⁴V. A. Sabelnikov, A. N. Lipatnikov, N. Nikitin, S. Nishiki, and T. Hasegawa, "Solenoidal and
423 potential velocity fields in weakly turbulent premixed flames," Proc. Combust. Inst. **38**, 3087 (2021).
- 424 ³⁵A. S. Monin and A. M. Yaglom, *Statistical Fluid Mechanics: Mechanics of Turbulence*, vol. 2 (MIT
425 Press, Cambridge, Massachusetts, 1971).
- 426 ³⁶A. N. Kolmogorov, "Local structure of turbulence in an incompressible fluid at very high Reynolds
427 numbers," Dokl. Akad. Nauk SSSR **30**, 299 (1941).
- 428 ³⁷M. Lesieur, O. Metais, and P. Comte, *Large-Eddy Simulations of Turbulence* (Cambridge University
429 Press, Cambridge, U.K., 2005).

This is the author's peer reviewed, accepted manuscript. However, the online version of record will be different from this version once it has been copyedited and typeset.

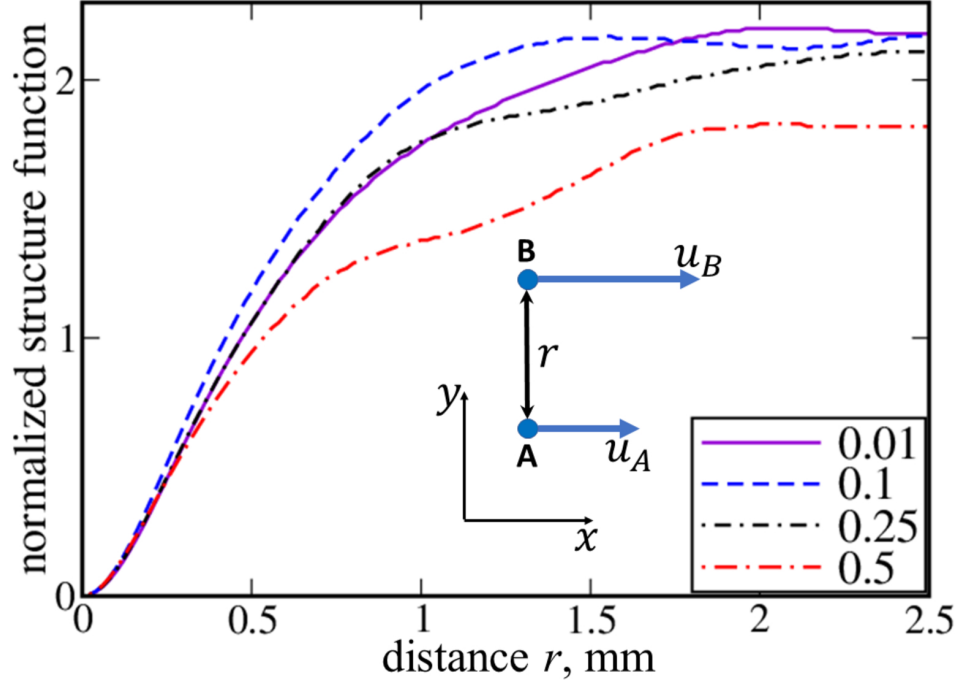
PLEASE CITE THIS ARTICLE AS DOI: 10.1063/5.0096509

Accepted to Phys. Fluids 10.1063/5.0096509

- 430 ³⁸M. P. Burke, M. Chaos, Y. Ju, F. L. Dryer, and S. J. Klippenstein, "Comprehensive H₂/O₂ kinetic
431 model for high-pressure combustion," *Int. J. Chem. Kinet.* **44**, 444 (2012).
- 432 ³⁹R. S. Rogallo, Numerical experiments in homogeneous turbulence, NASA Technical Memorandum
433 81315, NASA Ames Research Center, California, 1981.
- 434 ⁴⁰T. Passot and A. Pouquet, "Numerical simulation of compressible homogeneous flows in the turbulent
435 regime," *J. Fluid Mech.* **181**, 441 (1987).
- 436 ⁴¹N. Peters, *Turbulent Combustion* (Cambridge Univ. Press, Cambridge, UK, 2000).
- 437 ⁴²Ya. B. Zel'dovich, G. I. Barenblatt, V. B. Librovich, and G. M. Makhviladze, *The Mathematical*
438 *Theory of Combustion and Explosions* (Consultants Bureau, New York, 1985).
- 439 ⁴³Y. A. Gostintsev, A. G. Istratov, and Y. V. Shulenin, "Self-similar propagation of a free turbulent
440 flame in mixed gas mixtures," *Combust. Explos. Shock Waves* **24**, 563 (1988).
- 441 ⁴⁴B. D. Videto and D. A. Santavicca, D.A., "Flame-turbulence interactions in a freely-propagating,
442 premixed flame," *Combust. Sci. Technol.* **70**, 47 (1990).
- 443 ⁴⁵J. Furukawa, Y. Noguchi, T. Hirano, and F. Williams, "Anisotropic enhancement of turbulence in
444 large-scale, low-intensity turbulent premixed propane-air flames," *J. Fluid Mech.* **462**, 209 (2002).

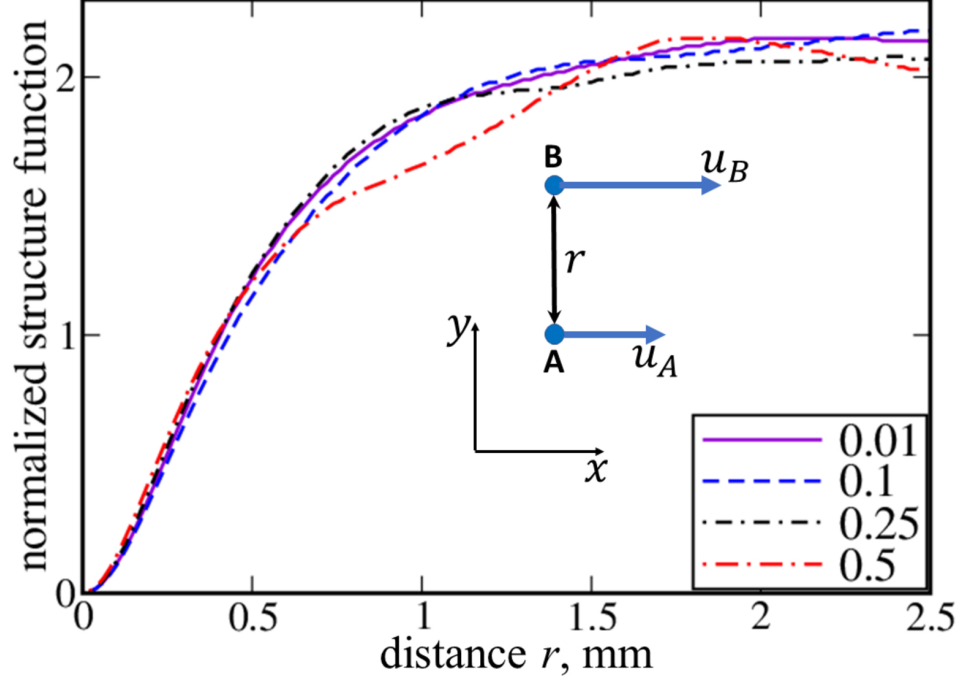
This is the author's peer reviewed, accepted manuscript. However, the online version of record will be different from this version once it has been copyedited and typeset.

PLEASE CITE THIS ARTICLE AS DOI: 10.1063/5.0096509



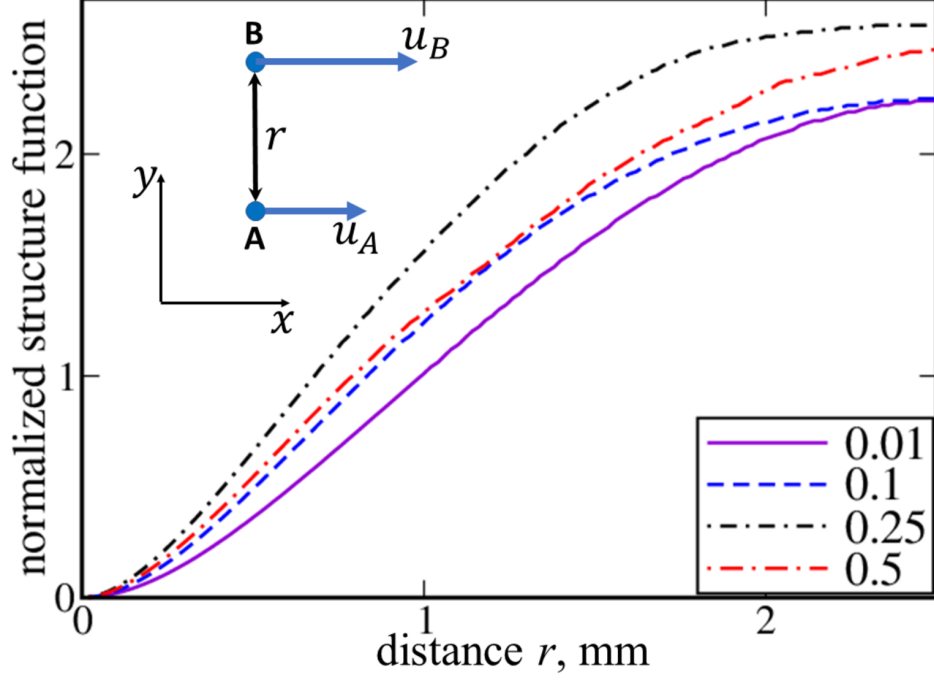
This is the author's peer reviewed, accepted manuscript. However, the online version of record will be different from this version once it has been copyedited and typeset.

PLEASE CITE THIS ARTICLE AS DOI: 10.1063/5.0096509



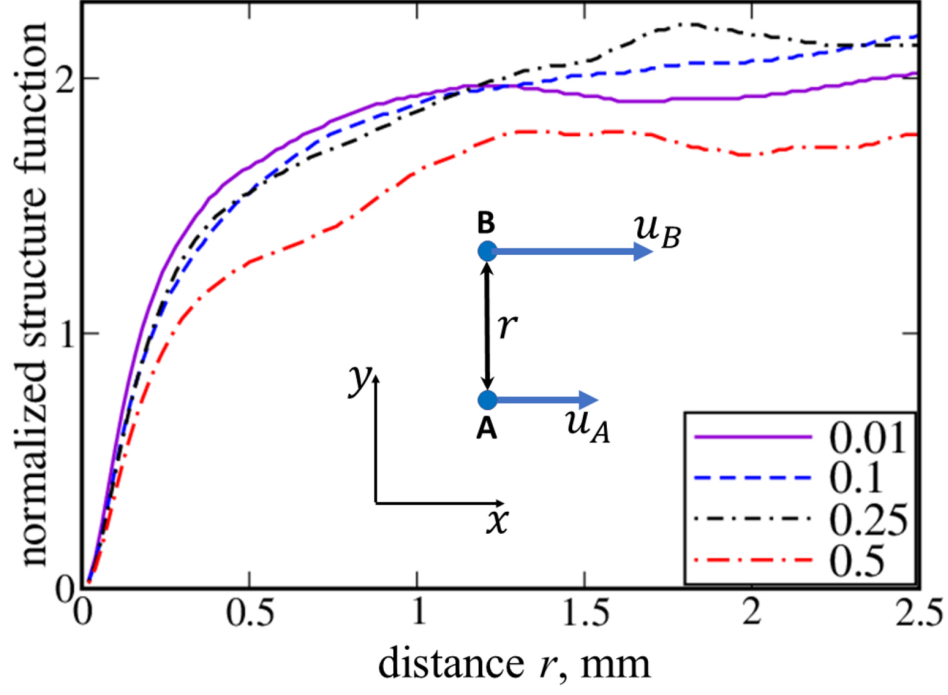
This is the author's peer reviewed, accepted manuscript. However, the online version of record will be different from this version once it has been copyedited and typeset.

PLEASE CITE THIS ARTICLE AS DOI: 10.1063/5.0096509



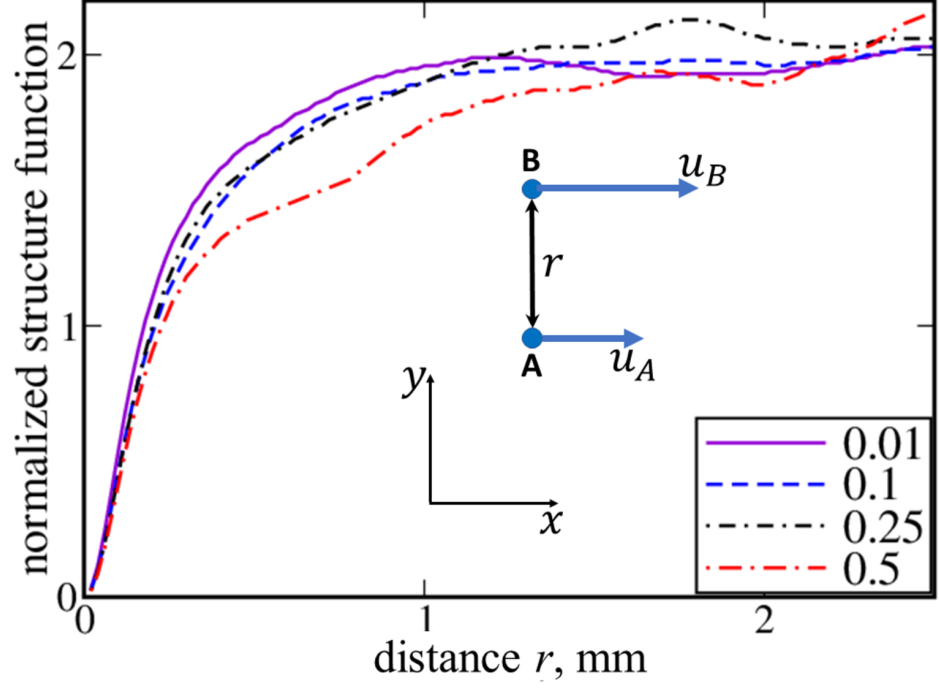
This is the author's peer reviewed, accepted manuscript. However, the online version of record will be different from this version once it has been copyedited and typeset.

PLEASE CITE THIS ARTICLE AS DOI: 10.1063/5.0096509



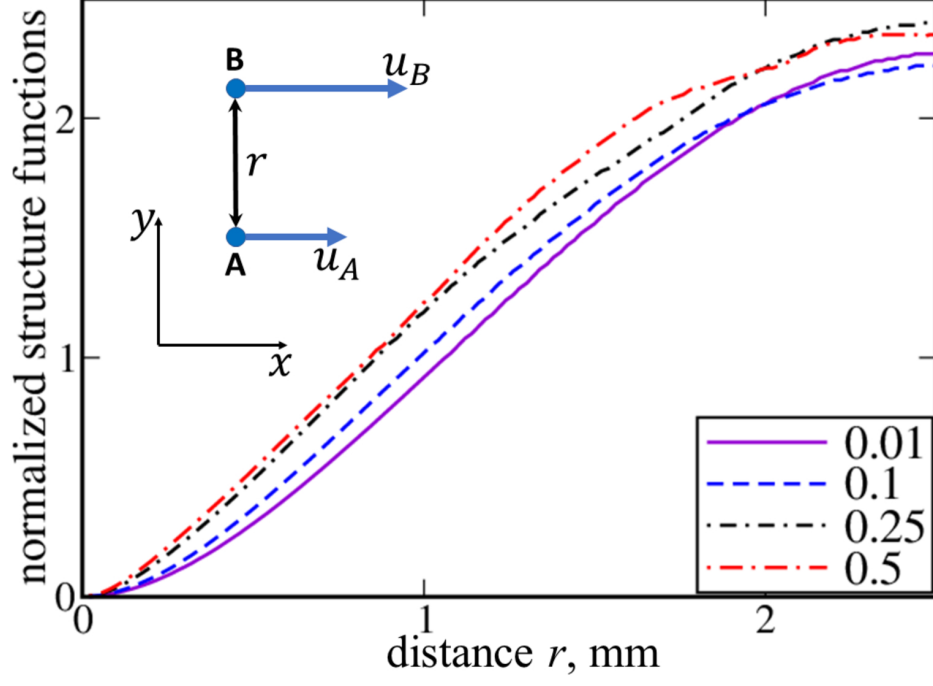
This is the author's peer reviewed, accepted manuscript. However, the online version of record will be different from this version once it has been copyedited and typeset.

PLEASE CITE THIS ARTICLE AS DOI: 10.1063/5.0096509



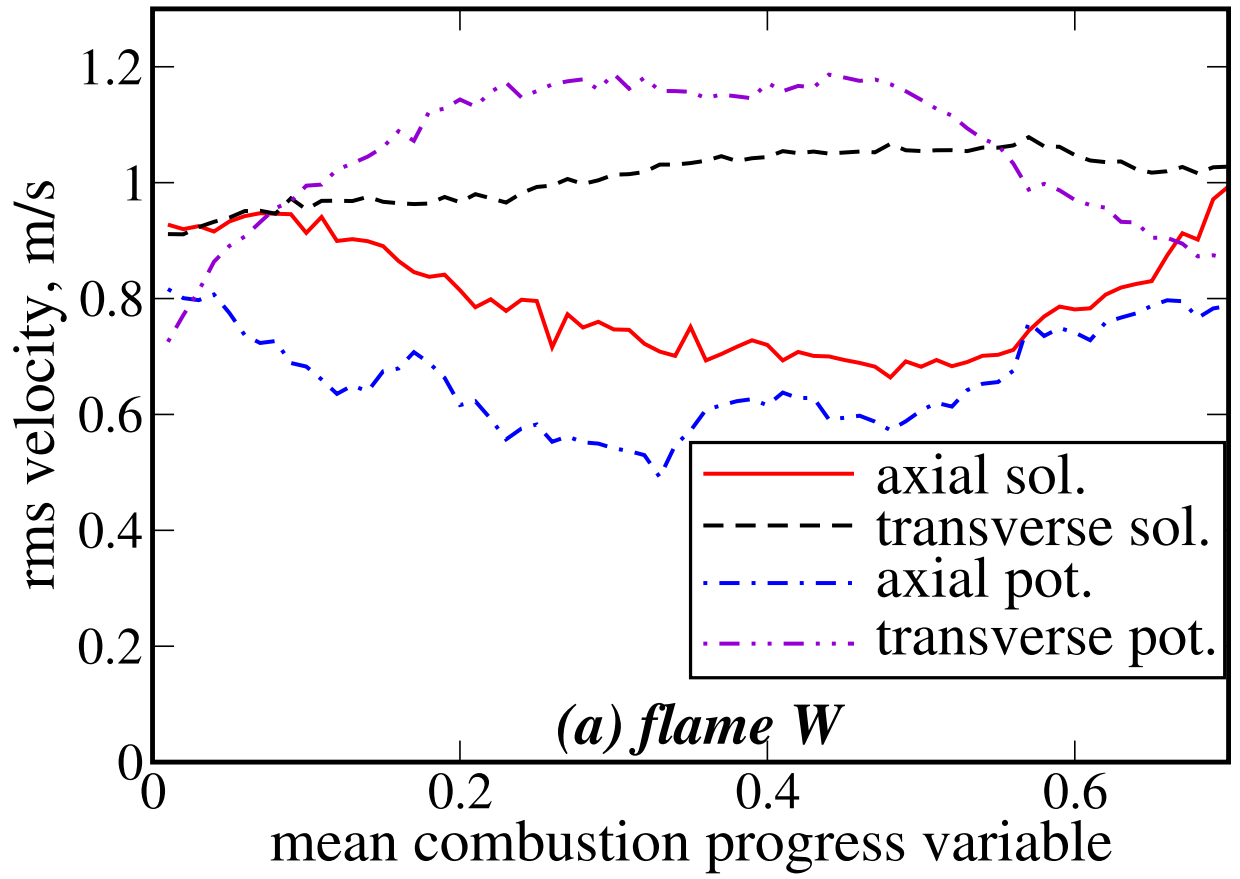
This is the author's peer reviewed, accepted manuscript. However, the online version of record will be different from this version once it has been copyedited and typeset.

PLEASE CITE THIS ARTICLE AS DOI: 10.1063/5.0096509



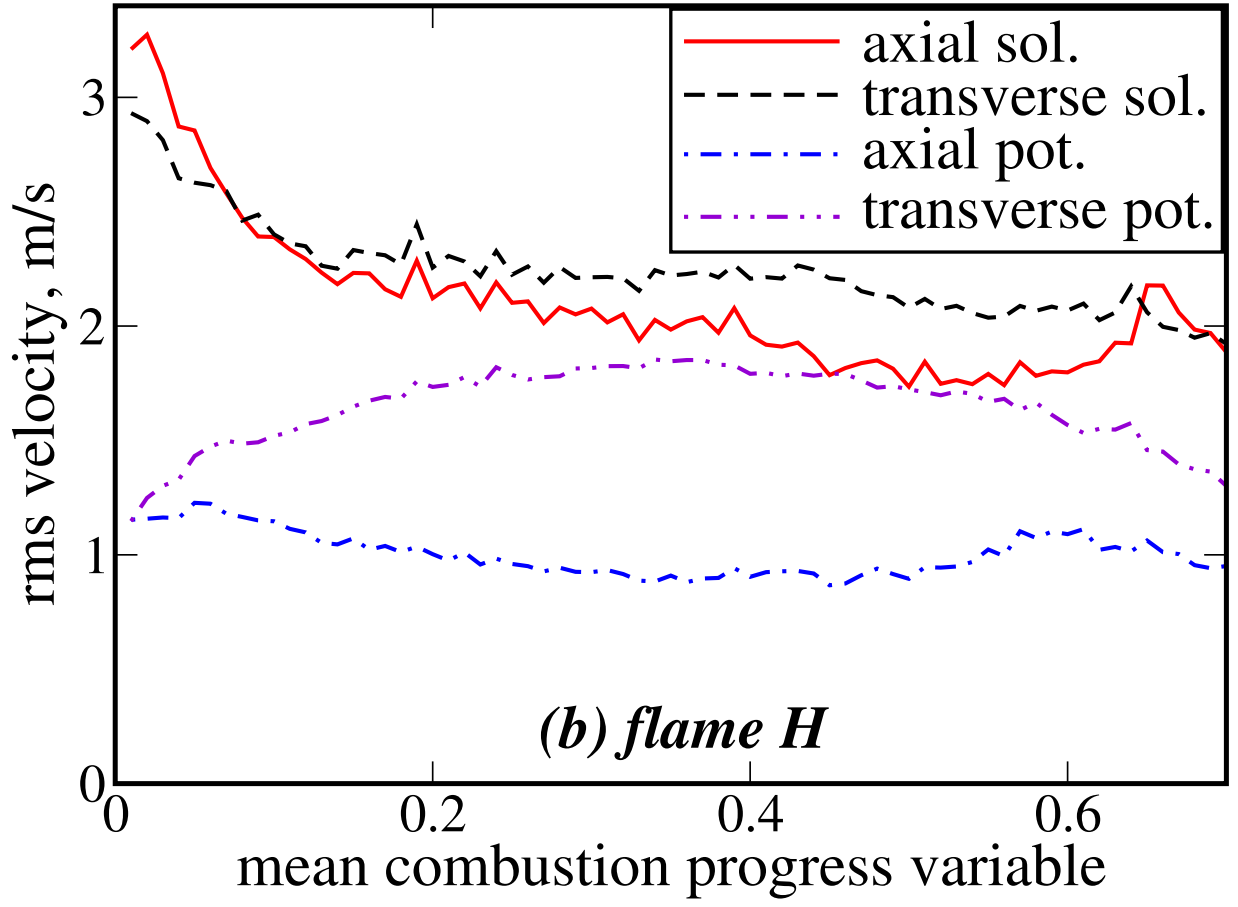
This is the author's peer reviewed, accepted manuscript. However, the online version of record will be different from this version once it has been copyedited and typeset.

PLEASE CITE THIS ARTICLE AS DOI: 10.1063/5.0096509



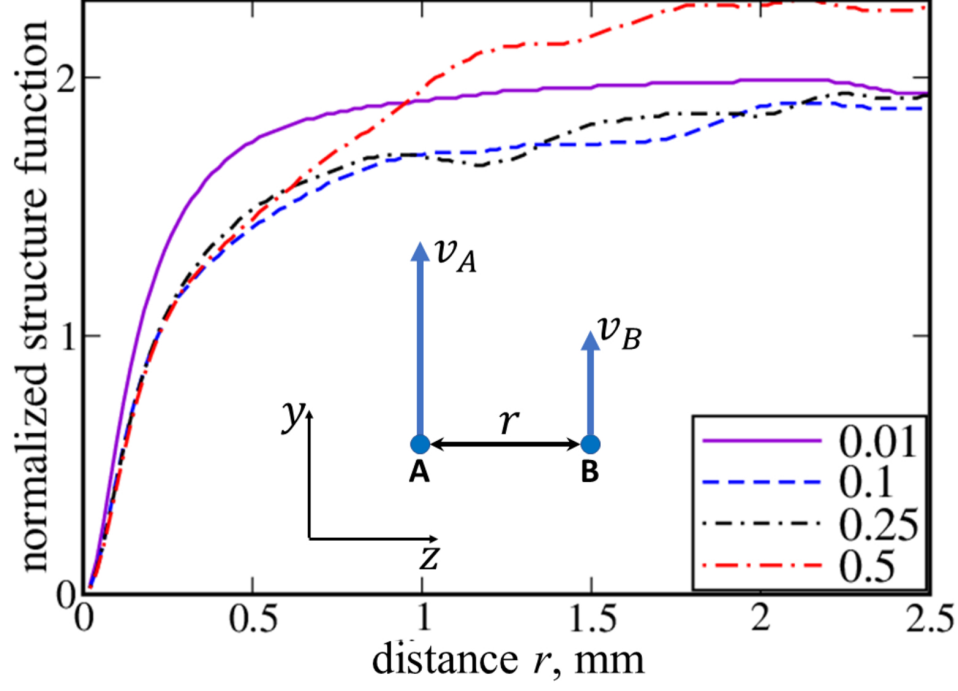
This is the author's peer reviewed, accepted manuscript. However, the online version of record will be different from this version once it has been copyedited and typeset.

PLEASE CITE THIS ARTICLE AS DOI: 10.1063/5.0096509



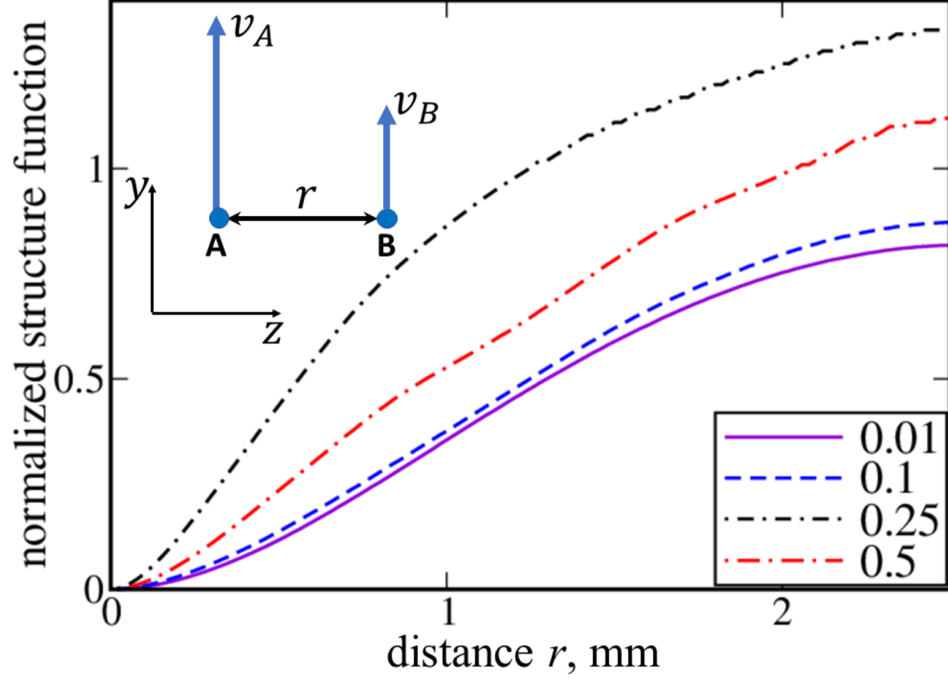
This is the author's peer reviewed, accepted manuscript. However, the online version of record will be different from this version once it has been copyedited and typeset.

PLEASE CITE THIS ARTICLE AS DOI: 10.1063/5.0096509



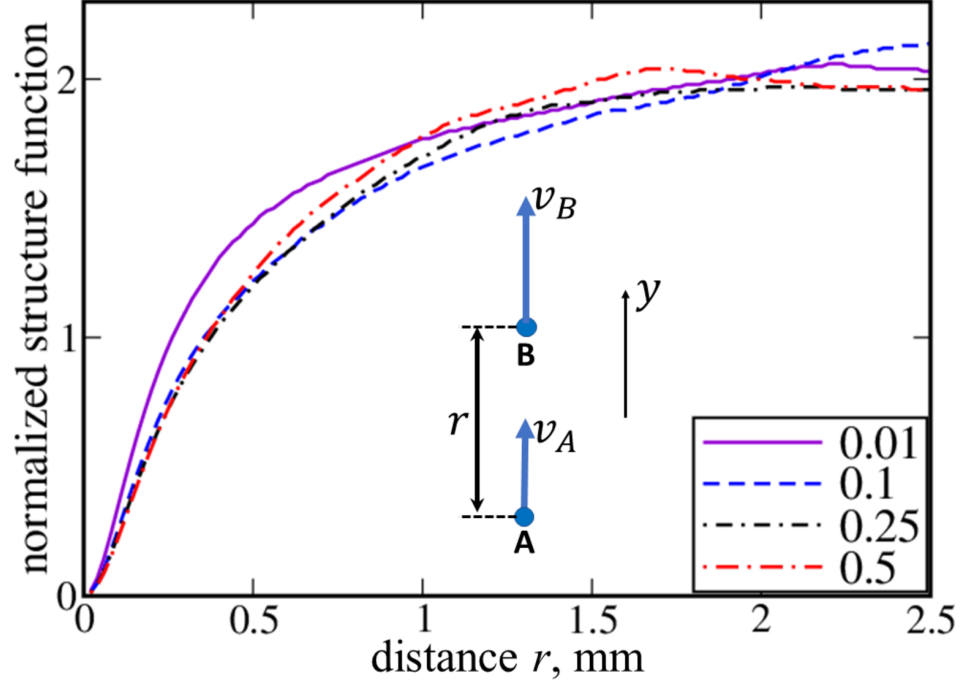
This is the author's peer reviewed, accepted manuscript. However, the online version of record will be different from this version once it has been copyedited and typeset.

PLEASE CITE THIS ARTICLE AS DOI: 10.1063/5.0096509



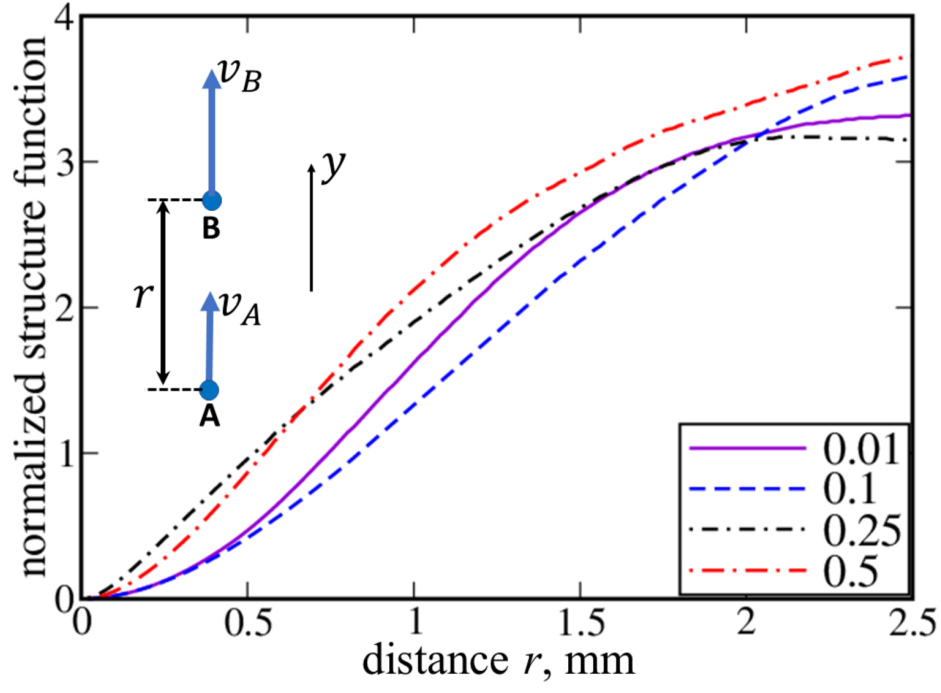
This is the author's peer reviewed, accepted manuscript. However, the online version of record will be different from this version once it has been copyedited and typeset.

PLEASE CITE THIS ARTICLE AS DOI: 10.1063/5.0096509



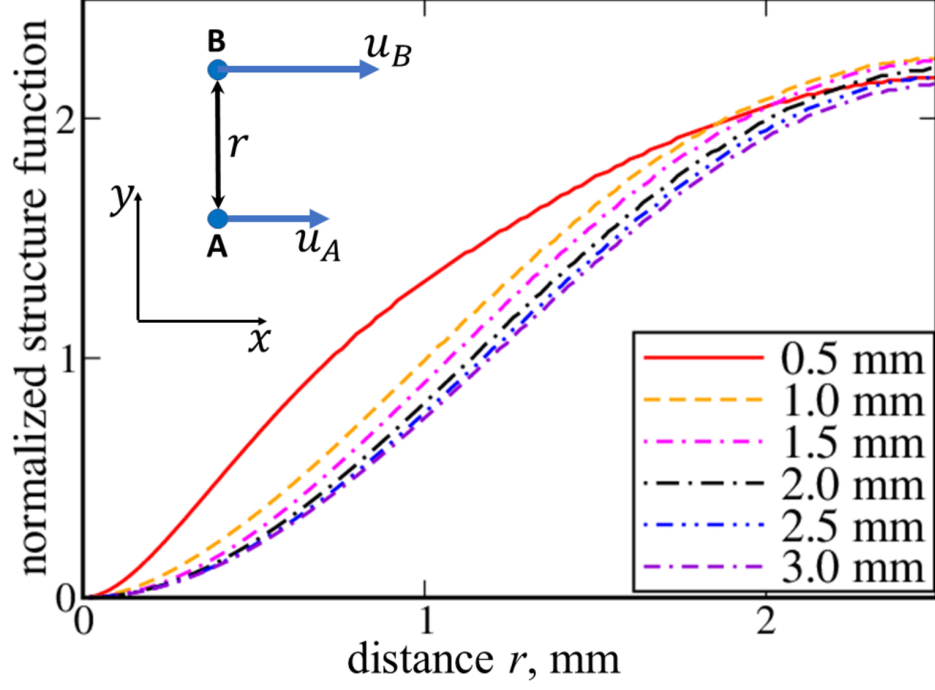
This is the author's peer reviewed, accepted manuscript. However, the online version of record will be different from this version once it has been copyedited and typeset.

PLEASE CITE THIS ARTICLE AS DOI: 10.1063/5.0096509



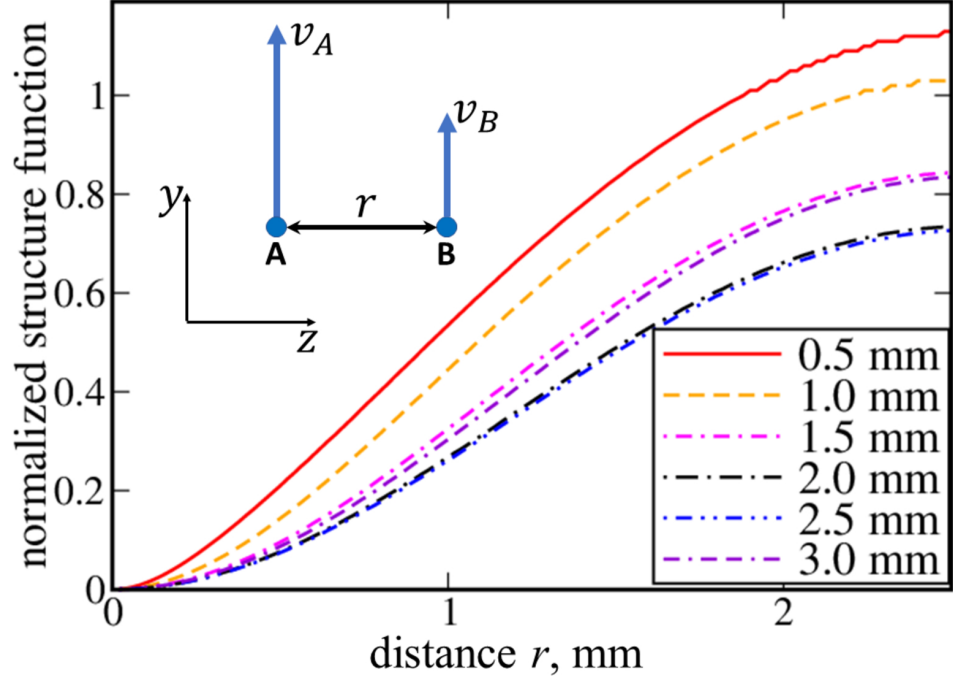
This is the author's peer reviewed, accepted manuscript. However, the online version of record will be different from this version once it has been copyedited and typeset.

PLEASE CITE THIS ARTICLE AS DOI: 10.1063/5.0096509



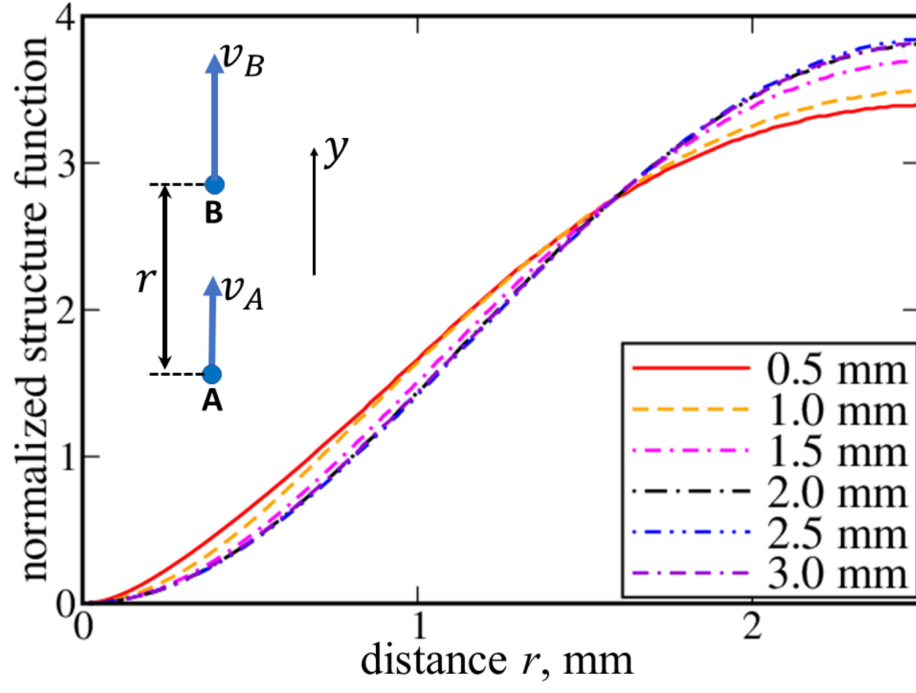
This is the author's peer reviewed, accepted manuscript. However, the online version of record will be different from this version once it has been copyedited and typeset.

PLEASE CITE THIS ARTICLE AS DOI: 10.1063/5.0096509



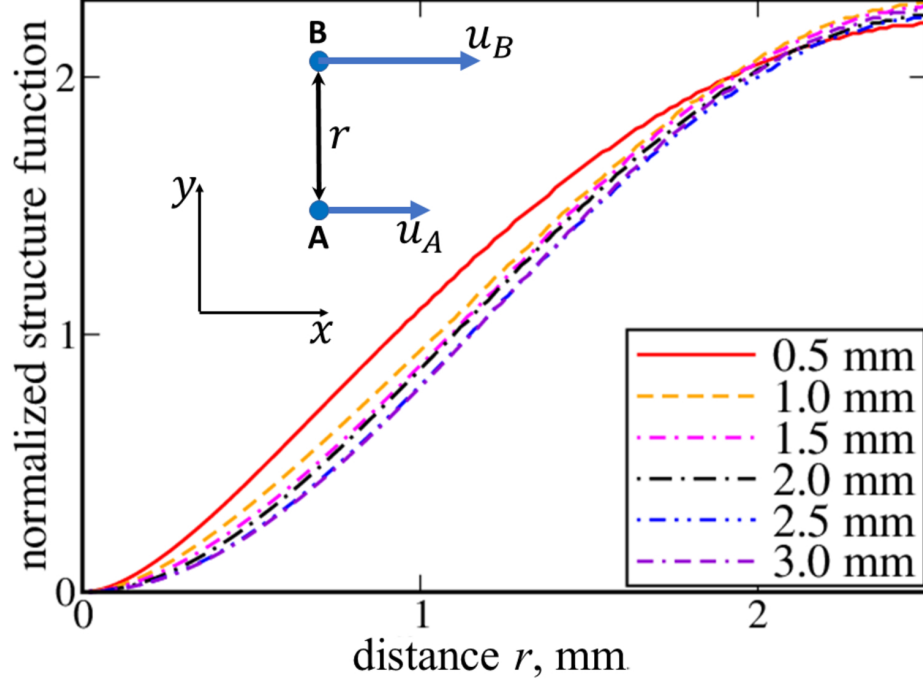
This is the author's peer reviewed, accepted manuscript. However, the online version of record will be different from this version once it has been copyedited and typeset.

PLEASE CITE THIS ARTICLE AS DOI: 10.1063/5.0096509



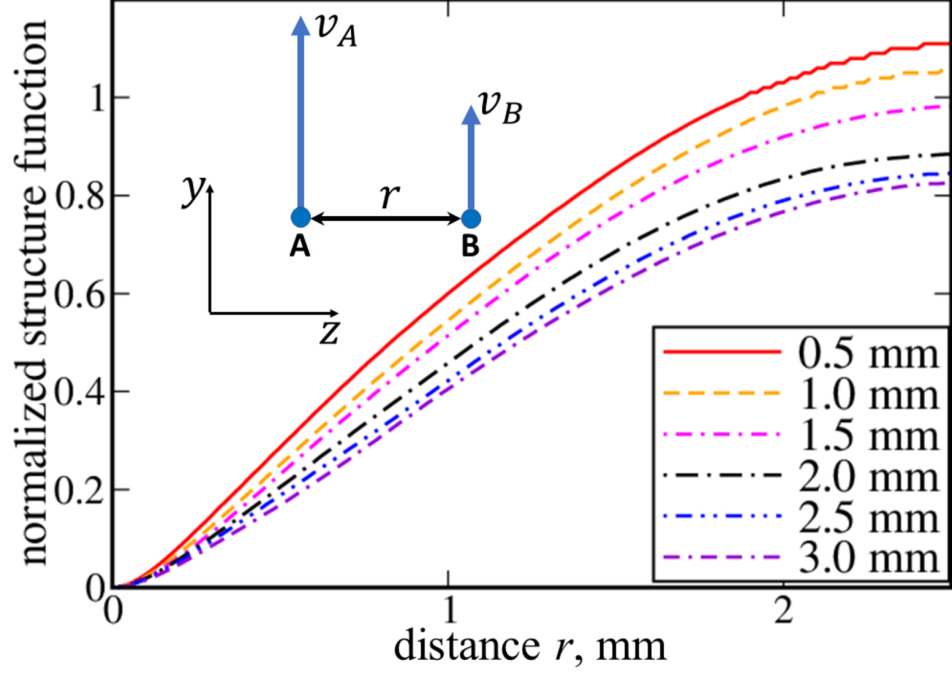
This is the author's peer reviewed, accepted manuscript. However, the online version of record will be different from this version once it has been copyedited and typeset.

PLEASE CITE THIS ARTICLE AS DOI: 10.1063/5.0096509



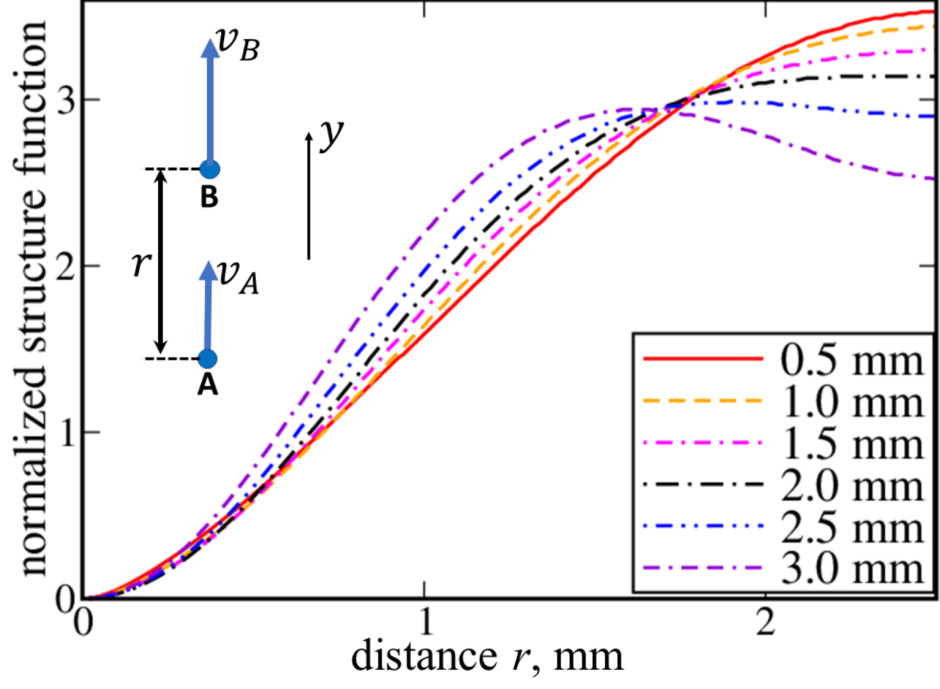
This is the author's peer reviewed, accepted manuscript. However, the online version of record will be different from this version once it has been copyedited and typeset.

PLEASE CITE THIS ARTICLE AS DOI: 10.1063/5.0096509



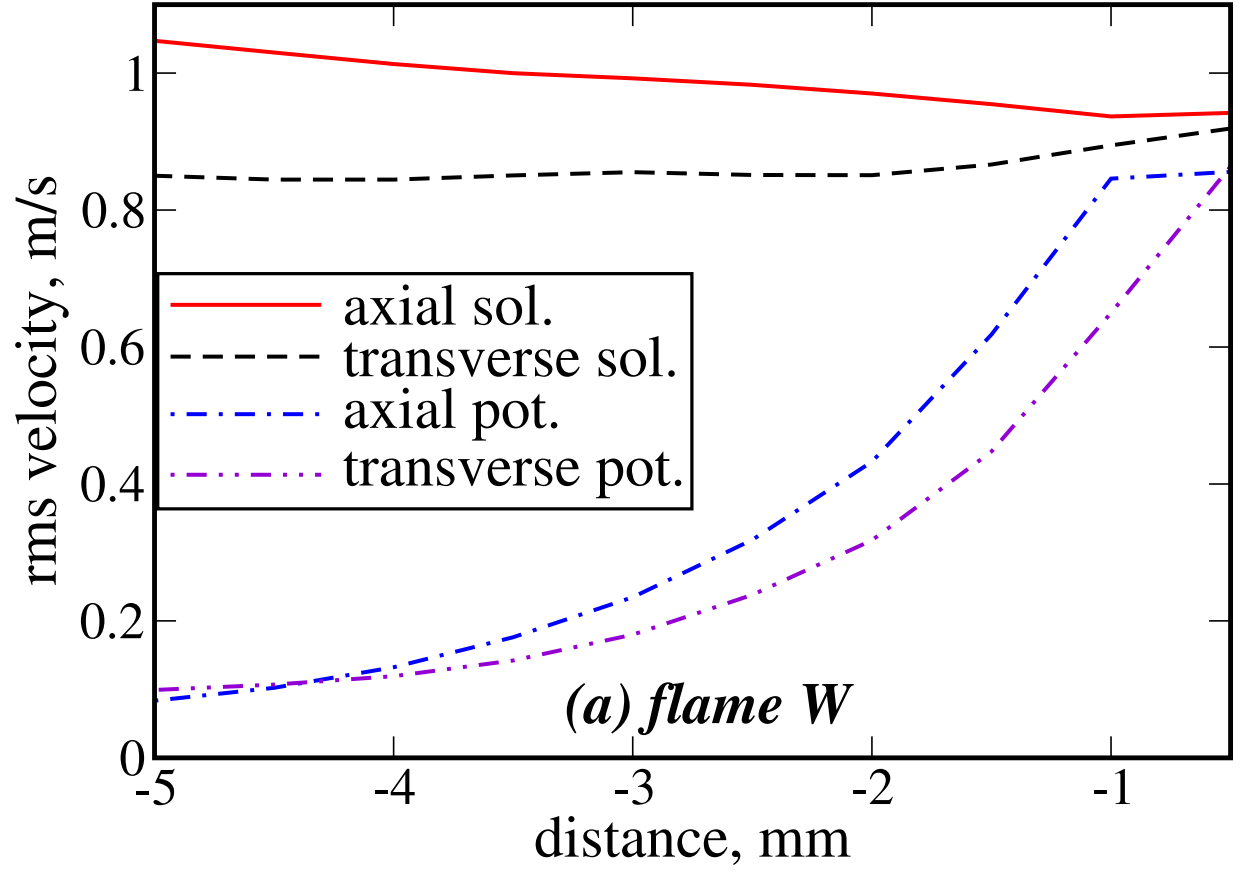
This is the author's peer reviewed, accepted manuscript. However, the online version of record will be different from this version once it has been copyedited and typeset.

PLEASE CITE THIS ARTICLE AS DOI: 10.1063/5.0096509



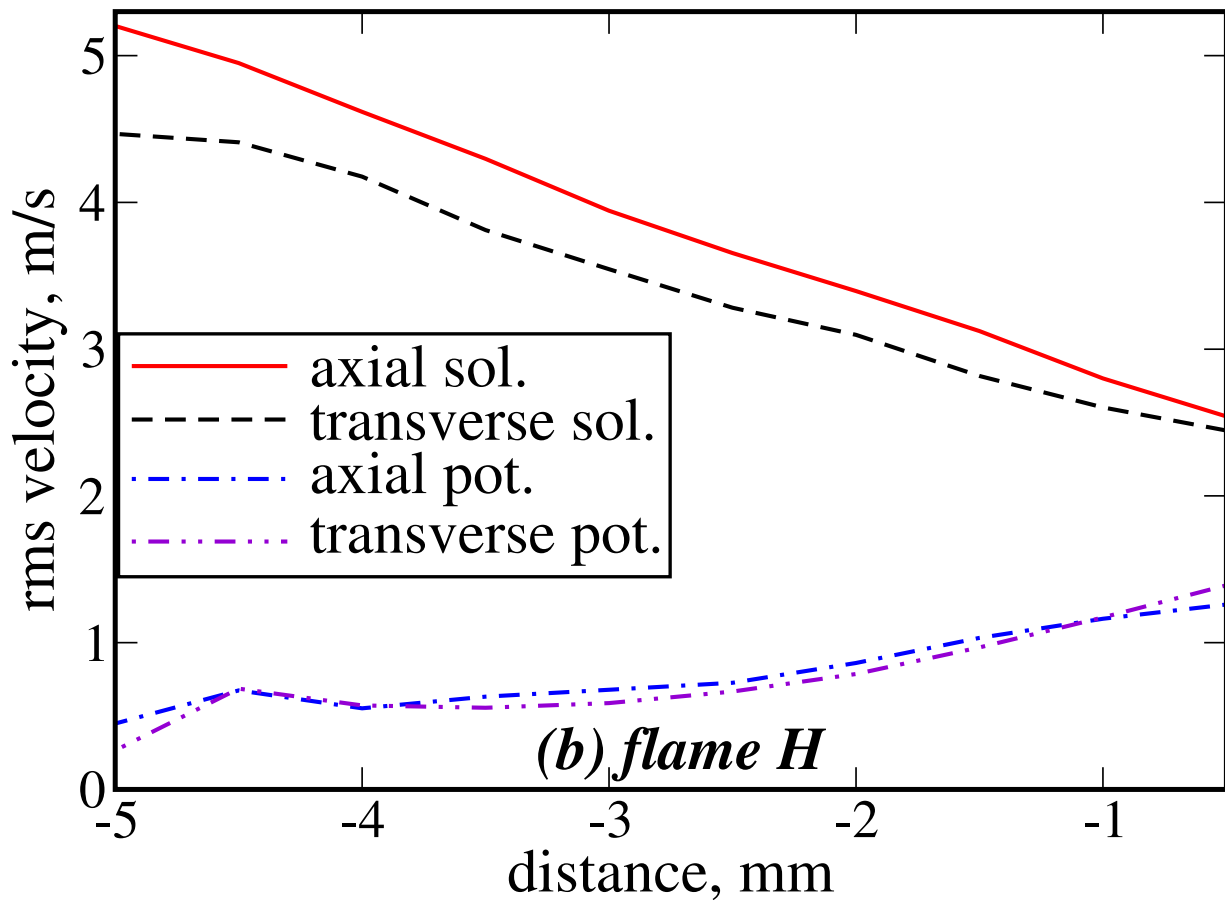
This is the author's peer reviewed, accepted manuscript. However, the online version of record will be different from this version once it has been copyedited and typeset.

PLEASE CITE THIS ARTICLE AS DOI: 10.1063/5.0096509



This is the author's peer reviewed, accepted manuscript. However, the online version of record will be different from this version once it has been copyedited and typeset.

PLEASE CITE THIS ARTICLE AS DOI: 10.1063/5.0096509



This is the author's peer reviewed, accepted manuscript. However, the online version of record will be different from this version once it has been copyedited and typeset.

PLEASE CITE THIS ARTICLE AS DOI: 10.1063/5.0096509

